Constraining the Mechanism and Kinetics of OH + NO_2 and HO_2 + NO Using the Multiple-Well Master Equation†

Jieyuan Zhang and Neil M. Donahue*

Department of Chemistry and Chemical Engineering, Carnegie Mellon University, Doherty Hall 1107, 5000 Forbes Avenue, Pittsburgh, Pennsylvania 15213

Received: October 4, 2005; In Final Form: March 15, 2006

Several recent experimental studies have provided substantial new constraints for the mechanisms on the HNO_3 potential energy surface. These include observations of biexponential OH decay over short time scales from OH + NO_2, which constrain key properties of the short-lived HOONO intermediate, observations of both conformers of the HOONO intermediate itself, isotopic scrambling data for ^{18}OH + NO_2, and observations of $HONO_2$ production from the HO_2 + NO reaction. We combine all of these recent data in a master-equation simulation of the system. This simulation is initialized with computational values for both stable species (wells) and transition states, but parameters are then adjusted to fit the observations. All parameters are kept within limits defined by experimental and theoretical uncertainty, and all converge away from their bounds. The primary fitting is carried out on the OH kinetic data—we first fit the biexponential kinetics, then address the isotopic scrambling. Isotopic scrambling is shown to be rapid but not complete at low pressure, while at least two parameter sets are shown to be consistent with the biexponential data. Of these two parameter sets, one is far more consistent with recent observations of *trans*-HOONO decay, isotopic scrambling, and $HONO_2$ production from HO_2 + NO. This we regard as the most probable potential energy surface for the reaction. On this PES, cis−trans isomerization for HOONO is slow but isomerization of *trans*-HOONO to $HONO_2$ is rapid. This has significant implications for observed HOONO behavior and also $HONO_2$ formation in the atmosphere from both HO_2 + NO and OH + NO_2.

1. Introduction

The OH + NO_2 reaction, forming nitric acid ($HONO_2$), is critically important to radical chain termination in tropospheric chemistry and radical sequestration in stratospheric chemistry.[1−3] However, it has now been confirmed that a minor channel leading to peroxynitrous acid (HOONO) formation has a branching ratio approaching 15% at STP.[4−7] This minor channel reveals itself in several ways: through biexponential OH kinetics[6,8] (HOONO can decompose on the time scale of some kinetics experiments), through ^{18}OH isotopic scrambling experiments[5,8] (H atom migration is possible in $HONO_2$ but not in HOONO), and through direct observation of HOONO products.[9−12]

In addition, the reaction of HO_2 + NO proceeds over the same potential energy surface (PES) as OH + NO_2, though with much higher initial energy. It is almost certain that HOONO is a vital intermediate in this reaction.[13] The HO_2 + NO reaction and the analogous RO_2 + NO reactions involving organoperoxy radicals play a vital role in the formation of ozone in the troposphere,[3] and the production of nitric acid and nitrates via both the OH + NO_2 and RO_2 + NO reactions is the major loss or sequestration pathway for NO_x. In sum, the PES for this system is arguably the most important in atmospheric chemistry.

Despite an extensive experimental data set[6,8,14−20] and considerable theoretical study[4,7,21−25] for the reaction OH + NO_2, many properties still remain uncertain for this reaction. It is widely accepted that there are some stable conformers of HOONO formed from the reaction OH + NO_2.[6,7,13,24−31] The two most stable conformers are *trans*−*perp*- and *cis*−*cis*-HOONO, with the key conformation being the orientation of the O−O−N−O moiety (trans or cis). Many of the critical unsolved problems in this family of reactions relate to the behavior of these conformers; these include the extent to which either conformer can be formed directly from the OH (or RO) + NO_2 precursors, the extent of interconversion of the two conformers under typical conditions, and the extent to which either conformer can isomerize directly to the nitrate ($HONO_2$ or $RONO_2$). Nitrate formation in particular is of enormous importance; only once the system reaches this very stable minimum can we assume that true radical chain termination has occurred.

We have previously considered the formation of organic nitrates in the RO_2 + NO reaction, focusing on larger secondary peroxy radicals where we could reasonably assume that the PES remained effectively constant with changing carbon number.[13,24] In that work, we showed that organic nitrate yield data covering a wide range of pressures, temperatures, and carbon numbers were consistent with two key assumptions about the nature of the full PES: first, interconversion of the *cis*- and *trans*-ROONO conformers was taken to be relatively slow; and second, only one of the conformers was taken to isomerize readily to $RONO_2$ (with a transition-state energy clearly lower than the separated RO + NO_2 products). Master-equation simulations based on this assumption showed good agreement with experimental nitrate yields. Furthermore, it was difficult to reproduce key aspects of the experimental data without these assumptions.

† Part of the special issue "David M. Golden Festschrift".

* To whom correspondence should be addressed. E-mail: umd@andrew.cmu.edu.

10.1021/jp0556512 CCC: $33.50
Published on Web 04/28/2006

Specifically, by separating the two conformers and allowing only one to lead to nitrate formation, we were able to understand low-temperature asymptotic nitrate yields of much less than unity (single-well ROONO simulations tend to shut down radical production entirely at low temperature and high pressure).

A key question is whether these conclusions extend to HNO_3. Several recent experimental results bear on this question. First, the isotopic scrambling and multiexponential kinetic data already mentioned exist for OH + NO_2 only. Second, nitric acid production at very low yields has been observed for the HO_2 + NO reaction.[32] Third, direct observations in a low-temperature flow reactor of *cis*- and *trans*-HOONO kinetics show rapid *trans*-HOONO decay.[12] These last data have been interpreted to show rapid isomerization between the *cis*- and *trans*-HOONO conformers but in fact show only that *some* rapid loss pathway exists for *trans*-HOONO. The same data also appear to show that both *cis*- and *trans*-HOONO are formed readily from the OH and NO_2 reactants.

A challenge for theoretical treatment of this system is that the transition states are difficult to constrain computationally. It is especially hard to locate a satisfactory transition state from ROONO to $RONO_2$ using ab initio calculations. Our approach has been to treat this as a free parameter, using the data to constrain the transition-state energy and frequencies (through the observed activation energy and A factor of the nitrate yields). The data speak clearly for organic nitrates; the critical energy for this transition state is substantially below the RO + NO_2 energy. However, the extent to which this conclusion holds for OH + NO_2 is an open question. It appears that most of the energies on the OH (and RO) + NO_2 PES are similar for all H and R except the OH (or RO) + NO_2 energy itself,[24] and it seems plausible that, if indeed the ROONO → $RONO_2$ isomerization transition state is defined by an almost broken RO−ONO bond, then this energy would be tied to but somewhat lower than the RO + NO_2 energy in general.

Aside from this difficult, loose transition state, the other energies in the potential energy surface for the OH + NO_2 reaction system are reported at different levels of theory with good agreement among them.[5,7,12,13,24,31,33] The second least-well constrained energy is the next-most important, the *cis*−*trans*-HOONO isomerization barrier, with density-functional calculations showing a higher rotational barrier than higher-level calculations. Finally, the formation of FONO isomers from F + NO_2 has been discussed from the perspective of a two-state avoided curve crossing by Ellison and co-workers;[34] these authors suggest that the formation of *cis*-XONO is essentially barrierless from X + NO_2 but that the formation of *trans*-XONO may have a significant formation barrier. The consequence would be that direct formation of *trans*-HOONO from OH + NO_2 would be negligible compared with the barrierless processes on the PES.

Another uncertainty for the OH + NO_2 reaction is the high-pressure limit for the rate constant. Smith et al. obtained a value of $(4.8 \pm 0.4) \times 10^{-11}$ cm^3 molecule^{-1} s^{-1} for k_∞ from measurements of OH($v = 1$) deactivation;[35] absolute kinetics in extreme pressures of He from Fulle and Hippler et al. extrapolate to $k_\infty = (5.2 \pm 2.2) \times 10^{-11}$ cm^3 molecule^{-1} s^{-1};[6,17,36] Donahue et al. obtained $k_\infty = (4.8 \pm 1.0) \times 10^{-11}$ cm^3 molecule^{-1} s^{-1} from a combined fit of available kinetic data, including multiple bath gas types;[16] and most recently, D'Ottone et al.[8] reported $k_\infty = (6.4 \pm 0.2) \times 10^{-11}$ cm^3 molecule^{-1} s^{-1}. Also, Troe obtained a value of 3.6×10^{-11} cm^3 molecule^{-1} s^{-1} for $HONO_2$ and 1.9×10^{-11} cm^3 molecule^{-1} s^{-1} for HOONO (thus a total of 5.5×10^{-11}) from his simulations;[23] Golden et al. published k_∞ as 2.7×10^{-11} cm^3 molecule^{-1} s^{-1} for $HONO_2$, 1.6×10^{-11} cm^3 molecule^{-1} s^{-1} for *cis*-HOONO, and 3.8×10^{-11} cm^3 molecule^{-1} s^{-1} for *trans*-HOONO (a total of 7.1×10^{-11}).[7] Although all of the values are consistently in the same range $(4.8-7.1) \times 10^{-11}$ cm^3 molecule^{-1} s^{-1}, the residual uncertainty is 50%. Furthermore, the high-pressure limits for the specific product formation channels are not well-known.

Additional information on the reaction dynamics has come from isotopic scrambling data using ^{18}OH + NO_2.[5,8,37,38] The simple notion motivating these experiments is that the H-atom may be free to migrate from oxygen to oxygen in $HONO_2$ but certainly will not be free to do so in HOONO. Migration of the H atom leads to scrambling of the ^{18}O in $HONO_2$, and subsequent decomposition of the $HONO_2$ would lead to OH + ^{18}ONO 67% of the time for complete scrambling. In this event, a low-pressure measurement of the effective ^{18}OH disappearance kinetics would reveal a value equal to 2/3 k_∞ for the $HONO_2$ formation channel. However, there is doubt in the literature as to whether scrambling is indeed rapid in the nascent $HONO_2$ and thus whether the extrapolation to k_∞ is valid—recently, D'Ottone et al. suggested that scrambling was in fact incomplete. Furthermore, no study of isotopic scrambling has considered the possibility that some nascent HOONO might isomerize into $HONO_2$, thus leading to "secondary" scrambling.

Our objective is to simulate both biexponential and isotopic scrambling kinetics data with a multiple-well master-equation simulation. In so doing, we shall test the applicability of the basic PES developed in our earlier work for $RONO_2$ to the $HONO_2$ system; specifically, we shall focus on the questions of how rapid cis−trans isomerization is for HOONO, the most probable energy of the HOONO−$HONO_2$ isomerization transition state, and the competition between H atom scrambling and dissociation in isotopically labeled $HONO_2$. In so doing, we aim to test the general consistency of literature kinetic data with the key details of this PES.

2. Potential Energy Surface

We assume the OH + NO_2 reaction system reacts in the same manner as we described in early papers.[5,13] Specifically, we assume that the reaction proceeds over a single, adiabatic, ground-state PES shown in Figure 1. $HONO_2$ isotopic scrambling is only considered when we simulate ^{18}OH reacting with NO_2. When the reaction starts, $HONO_2$, *trans*-HOONO, and *cis*-HOONO are formed immediately from OH + NO_2 with $k_{\infty,HONO2}$, $k_{\infty,trans-HOONO}$, and $k_{\infty,cis-HOONO}$, respectively. *trans*-HOONO has four reaction pathways: it dissociates to HO_2 + NO or OH + NO_2, and it isomerizes to *cis*-HOONO or $HONO_2$. *cis*-HOONO has three reaction pathways: it dissociates to HO_2 + NO or OH + NO_2, and it isomerizes to *trans*-HOONO (it cannot isomerize to $HONO_2$). $HONO_2$ has three reaction pathways: it dissociates to OH + NO_2, it isomerizes to *trans*-HOONO, and it undergoes H scrambling (when we consider ^{18}OH reacting with NO_2, H(^{18}O)NO_2 isomerizes to HON(^{18}O)O). In total, there are five stable species, five dissociation reactions, and three isomerization transition states in the entire HNO_3 reaction system, with the details shown in Figure 1.

Some features of this PES originated as phenomenological assumptions in our earlier work. Specifically, we assumed that both HOONO conformers coupled easily to OH + NO_2 but that only one could easily isomerize to $HONO_2$. We chose *trans*-HOONO for this second role based entirely on appearance; visual inspection suggests that it is easier for *trans*-HOONO to execute a modest in-plane rotation to $HONO_2$ than it is for *cis*-

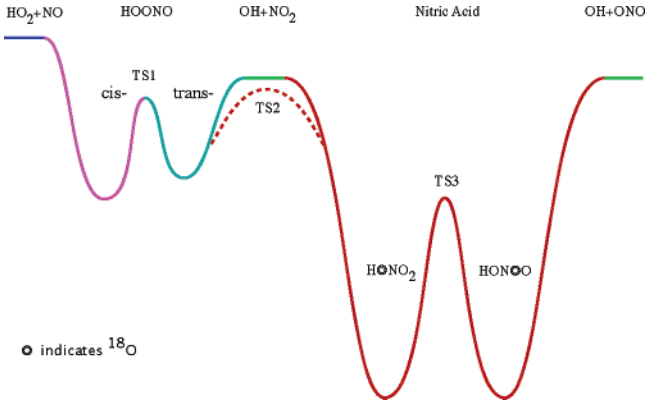

Figure 1. Potential energy surface and key species involved in the OH + NO_2 reaction system. The energies used in this study are shown in Table 1. There are five stable species, five dissociation reactions, and three other transition states in the whole OH + NO_2 reaction system: (HO_2 + NO), *cis*-HOONO, *trans*-HOONO, (OH + NO_2), and $HONO_2$; the transition state between *trans*-HOONO and *cis*-HOONO (TS1), the transition state between *trans*-HOONO and $HONO_2$ (TS2), the transition state between H(^{18}O)NO_2 and HON(^{18}O)O in the ^{18}OH + NO_2 simulation (TS3). Note that OH + NO_2 and HO_2 + NO lead to both *cis*- and *trans*-HOONO directly.

HOONO to execute something of a barrel-roll to $HONO_2$. Our firm conclusion was and is that there is no reason to expect these two isomerization energies to be similar, and for the sake of clarity, we took one pathway to be open and one to be closed. It should also be noted that this purely adiabatic, ground-state picture certainly neglects any important role for low-lying excited states or weakly avoided curve crossings.

Recent evidence for the OH + NO_2 system appears to support most of our assumptions. Fry et al.[12] observed large initial yields of both conformers from OH + NO_2, suggesting that indeed both formation channels are facile (even a small barrier for either channel would dramatically reduce the production rate for that pathway). At the same time, Fry et al.[12] observed rapid loss of *trans*-HOONO at 230 K, which they interpreted as the isomerization of *trans*-HOONO to *cis*-HOONO; however, it is equally possible that this loss is due to isomerization to $HONO_2$. Here, we shall argue that the weight of the evidence from both the HNO_3 and RNO_3 systems supports the hypothesis that both this specific feature (isomerization of *trans*-HOONO to $HONO_2$) and the general features of the PES shown in Figure 1 are substantially correct.

The energies for the OH + NO_2 reaction system, including the five stable species and the three transition states, are shown in Table 1. We use the energy of *cis*-HOONO as the reference energy. While this may seem to be an unusual choice, when one considers the homologous PESs for HNO_3 and RNO_3, the energies of most of the minima appear to be relatively consistent with the notable exception of the (OH + NO_2) "well", meaning that the OH or RO energy varies from surface to surface.[24] Consequently, the reactant energy for this specific reaction is not the best reference for considering the broader sequence of reactions, and we instead use *cis*-HOONO. Energies (shown in cm^{-1}) were calculated using B3LYP/6-31+G(d,p). Literature results for different levels of theory are also listed in the table for comparison.[5,7,13,24,31] Our results are generally consistent with the literature.

A critical feature on this PES is the transition-state energy for $HONO_2$ isotopic scrambling (TS3 in Table 1). Our result is consistent with our early value,[5] but there are no computational results at a higher level of theory against which to compare the density-functional value. Another important issue on this PES is the isomerization transition state between *trans*-HOONO and $HONO_2$. We could not locate a stable geometry for the transition state between these two species in our computational work. The results from Zhao et al.[31] and Lohr et al.[24] differ by about 9500 cm^{-1}. As described in an early paper,[13] we obtained this critical energy (E_{TS2}) by analyzing nitrate yield data from the RO_2 + NO reaction (R is the alkyl group) for a series of R. That analysis showed that the isomerization transition state lies approximately 1530 cm^{-1} lower than the radical products (OH + NO_2). This value is close to the result by Zhao et al.[31] In the simulations presented, we use recently published OH biexponential decay data[6,8] to help constrain this value.

2.1. Subsystems for the Master Equation. Our objective is to simulate both multiexponential kinetics data and isotopic scrambling data. At first blush, these are separate issues, so we shall address them with a succession of multiple-well models, each with increased complexity. In all cases, bimolecular species will be treated as a "well", that is, assumed to be thermally equilibrated with a large excess of one reagent (typically NO_2).

(1) Three-well system: (OH + NO_2), HOONO, and $HONO_2$. The starting point for the analysis of biexponential kinetic data has been a three-well system with no conversion between HOONO and $HONO_2$.[6,8] This system can be solved analytically (for a single experiment), but the full time, pressure, and temperature dependence still requires a simulation. Least-squares fitting to the analytical functions from this simple system fits the data well and leads to sensible-seeming parameters; consequently, this serves as the natural starting point for our simulations. In this part, we use the geometry and energy of *cis*-HOONO for HOONO, we do not consider $HONO_2$ isotopic scrambling, but we do consider the conversion between HOONO and $HONO_2$.

(2) Four-well system: (OH + NO_2), *trans*-HOONO, *cis*-HOONO, and $HONO_2$. We separate the *trans*- and *cis*-HOONO

TABLE 1: Energies for the OH + NO_2 Reaction System[a]

HO_2 + NO	*cis*−*cis*-HOONO[b]	TS1[c]	*trans*−*perp*-HOONO	OH + NO_2	TS2[d]	$HONO_2$	TS3[e]	ref
7867	0	4680	745	5199		−10097		Zhang[13]
	0						−130	this work
	0	4440	770	4060	4160	−10910		Zhao[31]
	[0]	[4510]	[1120]	[6850]	[7380]	[−10420]		Zhao[31]
	0	4700	680	3790		−10790		Golden[7]
	(0)	(4970)	(1130)	(6090)		(−10160)		Golden[7]
7020	0			3790	13620	−10790		Lohr[24]
(9090)	(0)			(6080)		(−10160)		Lohr[24]
9090	0	5600	1050	6640		−10140	350	Donahue[5]

[a] Energies (shown in cm^{-1}) were calculated using B3LYP/6-31+G(d,p) (this work and Zhang et al.[13]), B3LYP/6-311++G** (by Zhao et al.,[31] Golden et al.,[7] and Lohr et al.[24]), B3LYP/6-31G** (by Donahue et al.[5]), CBS-QB3 (in square parentheses by Zhao et al.[31]), or G3 (in parentheses by Golden et al.[7] and Lohr et al.[24]). [b] All the energies are relative to the energy of *cis*−*cis*-HOONO intermediate. [c] Transition state between *trans*-HOONO and *cis*-HOONO. [d] Transition state between *trans*-HOONO and $HONO_2$. [e] Transition state for $HONO_2$ scrambling.

TABLE 2: Optimal Parameter Sets Obtained by the Three- and Four-well Master Equations and the Range and Step of the Parameters Used in the Simulation[a]

wells	$E_{cis-HOONO}$	E_{TS1}	$E_{trans-HOONO}$	E_{OH+NO2}	E_{TS2}	$k_{\infty,HONO2}$	$k_{\infty,c-HOONO}$	$k_{\infty,t-HOONO}$
		(cm^{-1})				(cm^3 molecule $^{-1}$ s^{-1})		
three	0			6400	6600	2.3×10^{-11}	4.3×10^{-11}	
min				6000	4400	2.0×10^{-11}	3.0×10^{-11}	
max				6900	7000	2.5×10^{-11}	5.0×10^{-11}	
step				25	50	0.1×10^{-11}	0.1×10^{-11}	
four	0	4800	750	6500	5900	2.3×10^{-11}	3.5×10^{-11}	1.5×10^{-11}
	0	**5500**	**950**	**6500**	**4700**	$\mathbf{2.2 \times 10^{-11}}$	$\mathbf{4.2 \times 10^{-11}}$	$\mathbf{1.0 \times 10^{-11}}$
min		4400	650	6000	4400	2.0×10^{-11}	3.0×10^{-11}	0.8×10^{-11}
max		5600	1250	6900	7000	2.5×10^{-11}	4.5×10^{-11}	2.0×10^{-11}
step		100	100	50	100	0.1×10^{-11}	0.1×10^{-11}	0.1×10^{-11}

[a] There are two sets of parameters for the four-well case. The overall optimum including consideration of $HONO_2$ yields from HO_2 + NO is shown in bold.

intermediates in this part, and we consider all transition states shown above except the isotopic scrambling. The primary objective in these simulations is to test the implications of including two distinct conformers of HOONO in the simulation. Specifically, the eigenvalues for the decomposition of the intermediates will be quite different, as calculations consistently reveal that *trans*-HOONO is some 1000 cm^{-1} less stable than *cis*-HOONO. The conclusions are certain to depend on whether cis−trans isomerization is rapid as well as the HOONO−$HONO_2$ isomerization energy. We also simulate the formation of $HONO_2$ from HO_2 + NO using this PES but with our nitrate yield model in which the radical species are not included as specific wells but rather as input or output channels.[13]

(3) Nine-well system: (OH + NO_2), *trans*-HOONO, *cis*-HOONO, $HONO_2$, (^{18}OH + NO_2), *trans*-H(^{18}O)ONO, *cis*-H(^{18}O)ONO, H(^{18}O)NO_2, and HON(^{18}O)O. In the "full" simulation, we consider the isotopic scrambling in particular, as well as the overall consistency of the PES.

For all of the OH + NO_2 simulations, to simplify the multiple-well master-equation simulations, we do not include HO_2 + NO bimolecular products. The reaction begins from OH + NO_2, and calculations show that the yields of HO_2 and NO from *trans*- and *cis*-HOONO are both below 1% under all conditions discussed here.

3. Theory

In this work, we shall combine computational results for stable species and transition states with master-equation simulations of the reaction dynamics, using the same basic procedures we have reported earlier.[13] The essential details follow, with extensive additional information in the Appendix and Supporting Information.

3.1. Microcanonical Rate Constants. We need to estimate the microcanonical rate constants for the various transition states shown in Figure 1. Structures and frequencies for all stable species are based on density-functional calculations (B3LYP/6-31+G(d,p)) as presented in the Table 1 and the Supporting Information. The microcanonical rate constants out of a given well are calculated by

$$k(E) = c\,\frac{G(E - E_0)}{\rho(E)} \qquad (1)$$

where $G(E - E_0)$ is the sum of states for the transition state at energy E with critical energy E_0 and $\rho(E)$ is the density of states for the well at the same energy E (in cm^{-1}). To calculate sums and densities of states, we used the Densum program developed by Barker.[39]

3.2. Master Equation. For statistical reaction dynamics, we employ the time-dependent master equation. The time-dependent one-well master equation has been described in detail in several previous references.[13,40,41] To treat the complex terrain of this reaction, we shall rely on the time-dependent multiple-well form of the matrix master equation, including canonical representations of the bimolecular species important to the reaction coordinate. We include the important bimolecular species in the simulation because it allows us to directly simulate a given set of experimental conditions quite easily. The advantage of explicit matrix inversion is that we can obtain explicit time-dependent solutions for all of the important species in the reaction; the limitation is computational time, but we are able to treat up to nine wells without excessive computational burdens. The details of the multiple-well matrix formalism are treated in Appendix 1; the important result here is that we obtain a full vector $\mathbf{N}(t)$ containing the energy-dependent population densities of all species in the simulation.

4. Results

4.1. Results from the Three-well Master-Equation Simulation. Our first objective is to use the three-well master equation to simulate the OH biexponential kinetics observed for the OH + NO_2 reaction, including results from Hippler et al.[6] and D'Ottone et al.[8] The setup and conditions are different for the two experiments: Hippler et al. conducted experiments at very high NO_2 concentration and very high pressure, while D'Ottone et al. conducted experiments with a series of lower NO_2 concentrations at normal pressure. The time scale in Hippler's experiment is thus 100 times smaller than that in D'Ottone's experiment. As we discuss in Appendix 1, in the multiple-well master equation dealing with dissociation and recombination, the NO_2 concentration should be much greater than OH concentration. We therefore place more weight on the data of Hippler et al. and the high-NO_2 data of D'Ottone et al. than the lower-NO_2 data of D'Ottone et al.

By including the HOONO−$HONO_2$ isomerization, our calculations differ from those presented earlier;[6,8] our objective is to investigate how low the TS2 energy can be and still be compatible with the observed biexponential kinetics. For this purpose, the TS2 energy is treated as a free parameter. Later, when we separate *cis*- and *trans*-HOONO, we shall see whether the constraints imposed by the kinetics are loosened.

We conducted an exhaustive search of possible values for E_{OH+NO2}, E_{TS2}, $k_{\infty,HONO2}$, and $k_{\infty,HOONO}$ to simulate the biexponential kinetics; the parameter range is set by the existing uncertainty in those values, so plausibility is also a constraint. The search range and step size of the parameters, as well as the optimal parameter values, are shown in Table 2. The reference

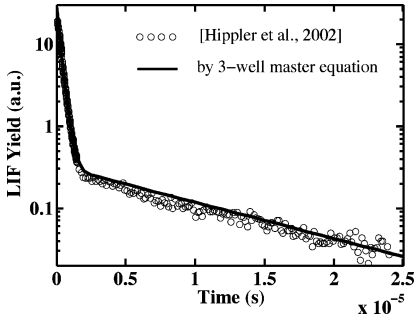

Figure 2. Simulation results by our three-well master equation for Figure 2 in Hippler et al.[6] The collision frequency ω is 1×10^{12} s^{-1}, $T = 430$ K, and $[NO_2] = 1.3 \times 10^{17}$ molecule cm^{-3}.

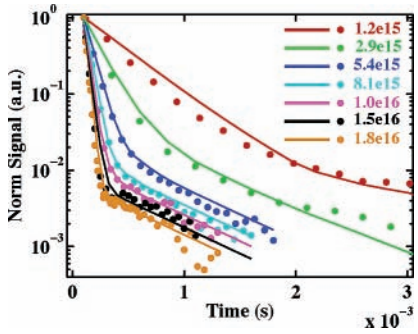

Figure 3. Simulation results by our three-well master equation for Figure 7 in D'Ottone et al.[8] The collision frequency ω is 5×10^9 s^{-1}, $T = 413$ K, and there are 7 sets of $[NO_2]$ ranging from 1.2×10^{15} to 1.8×10^{16} molecule cm^{-3}.

energy is E_{HOONO}, so E_{OH+NO2} is the HO−ONO bond strength. The collision frequency is calculated[42,43] using eqs 15−17 in our earlier work,[13] and E_{down} is fixed at 600 cm^{-1} for all the simulations. We first compare the simulation result with the data by Hippler et al. by minimizing the sum of the squares of the difference in the logarithm of the simulation and the data. We then use the parameter set at each minimum to simulate the data by D'Ottone et al.

We use a dual grain size for the energy levels in all the simulations, following the model of Barker—key regions near TS energies are modeled with a 50 cm^{-1} grain, and areas far from TS energies are modeled with a 150 cm^{-1} grain size. Due to the richness of the landscape, most of the energy space is modeled with a 50 cm^{-1} grain size. There is a modest improvement in the quality of fits with reduced grain size, but the increased computational costs in the larger models (especially the nine-well model) do not warrant performing all of the computations with a finer grain. A sensitivity analysis is presented in Appendix 2.

Figure 2 shows our simulation result for Figure 2 in Hippler et al., and Figure 3 shows our simulation result for Figure 7 in D'Ottone et al. Our simulation results agree well in each case, showing that a single set of parameters can indeed reproduce both data sets. The energies constrained by the data are consistent with our computational values shown in Table 1 except the energy for (OH + NO_2 − *cis*-HOONO), which agrees better with the calculation result by Donahue et al. at B3LYP/6-31G** and Golden et al. at G3.[5,7] The energy of (OH + NO_2) relative to the HOONO intermediate (6400 cm^{-1}) is slightly smaller than the experimental result by Hippler et al. (6930 ± 80 cm^{-1})[6] and the simulation result by Golden et al. (6800 cm^{-1}).[7]

The critical energy for the transition state from HOONO to $HONO_2$ (E_{TS2}) in the simulations is about 6600 cm^{-1} relative

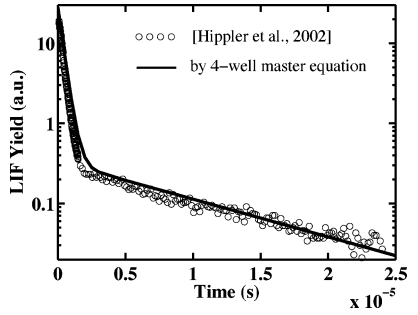

Figure 4. Simulation results by our four-well master equation for Figure 2 in Hippler et al.[6] The collision frequency ω is 1×10^{12} s^{-1}, $T = 430$ K, and $[NO_2] = 1.3 \times 10^{17}$ molecule cm^{-3}.

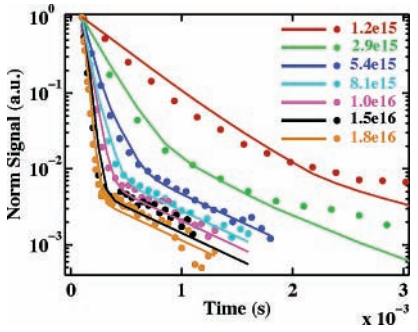

Figure 5. Simulation results by our four-well master equation for Figure 7 in D'Ottone et al.[8] The collision frequency ω is 5×10^9 s^{-1}, $T = 413$ K, and there are 7 sets of $[NO_2]$ ranging from 1.2×10^{15} to 1.8×10^{16} molecule cm^{-3}.

to the energy of HOONO, 200 cm^{-1} higher than the (OH + NO_2) energy. In this case, isomerization is secondary, as the dissociation pathway has higher entropy and thus always dominates (isomerization to $HONO_2$ is always less than 10% of dissociation back to reactants). The presence of the isomerization pathway does, however, lead to a better agreement between the simulations and the biexponential data, with a 24% reduction in the root-mean-square (rms) residuals. Consequently, for the three-well simulation, the biexponential data do not support extensive isomerization of HOONO to $HONO_2$, though they do suggest a modest role for this process.

4.2. Results from the Four-well Master-Equation Simulation. There is ample experimental and theoretical evidence for existence of at least two stable conformers of HOONO, so next we shall simulate the kinetic data taking into account these two conformers (*trans*- and *cis*-HOONO). The most pressing questions are the effect on the isomerization energy (E_{TS2}), the general influence of a third, very shallow well on the multiexponential kinetics, and the relative speed of isomerization between the two HOONO conformers.

The reaction mechanism is exactly the same as we specified in the PES section. There are now seven uncertain parameters that are important for the result: E_{OH+NO2}, $E_{trans-HOONO}$, E_{TS1} (the transition state energy for interconversion between *trans*- and *cis*-HOONO), E_{TS2}, $k_{\infty,HONO2}$, $k_{\infty,t-HOONO}$, and $k_{\infty,c-HOONO}$. Once again $E_{cis-HOONO}$ serves as the reference energy. As the number of wells in the multiple-well master equation increases, the calculation speed decreases dramatically and the number of free parameters increases. We again conduced an exhaustive search of parameter space under same procedure but with larger step sizes because of the computational cost.

The four-well simulation results are shown in Figure 4 and Figure 5. The fits are slightly less precise than in the three-well case (presumably because of the coarser step size), but the quality of the fits is still very high. For consistency with the

nine-well simulation, we have retained the 50 cm^{-1} fine energy grain size, but Figure 14 in Appendix 2 shows that a 10 cm^{-1} grain-size simulation improves the fit for the data from Hippler et al.

The optimal parameters for the four-well master equation, the search range, and step size of the parameters are also shown in Table 2. In this case, two fits are of similar quality; in each case, there is one low-energy barrier for the loss of *trans*-HOONO. In the first case (cis−trans coupling), $E_{TS1} < E_{TS2}$, and in the second case (*trans*-$HONO_2$ coupling), $E_{TS2} < E_{TS1}$. All the figures shown for the four-well simulations use the second parameter set. The energies constrained by the data and four-well master equation are generally consistent with the three-well simulation, with two notable exceptions. The most obvious difference is that the critical energy for TS2 (E_{TS2}) has dropped substantially in either case (by 700 or 1900 cm^{-1}) to a level well below the radical reactants. The lower TS2 energy is very close to the energy we obtained by analyzing the nitrate yield data from RO_2 + NO reactions for a series of R.[13] Much more isomerization to $HONO_2$ can be supported out of the shallow *trans*-HOONO well than out of a single HOONO well, regardless of the *cis*−*trans* HOONO isomerization barrier height. We thus see immediately that it is necessary to include both conformers to properly model the reaction dynamics. The second difference involves the total (*cis* + *trans*) HOONO formation rate constant (k_∞), which is larger than the three-well result in either case; this is because in both cases there is at least some dynamic separation between *cis*- and *trans*-HOONO.

Overall, the three- and four-well simulations are similar to each other and consistent with most computational constraints. It is not surprising that by separating *cis*- and *trans*-HOONO the simulations support a lower transition-state energy for isomerization to $HONO_2$, as the cis−trans isomerization in effect protects the double-exponential kinetics from the nitric acid well (which generates a pure single exponential with no thermal OH regeneration). We shall present a more detailed comparison with other experimental constraints in the discussion section.

4.3. Results from the Nine-well Master-Equation Simulation. Our next objective is to assess the role of isotopic (^{18}O) scrambling in this reaction. Specifically, we wish to assess the extent to which relatively low-pressure data constrain the high-pressure $HONO_2$ formation kinetics, the extent to which scrambling is complete at low pressures, and the potential for "leakage" from HOONO to $HONO_2$ to influence the scrambling kinetics. We will consider the full literature on the kinetics, which are not extensive.[5,8,37,38] The recent work of D'Ottone et al.[8] includes time-dependent data for both ^{18}OH and ^{16}OH, so we will focus primarily on these results. Those experiments employed an OH source producing around 50% ^{16}OH and 50% ^{18}OH, both of which react with NO_2. As a consequence, we must model the behavior of both ^{16}OH and ^{18}OH, which then couple through scrambling.

To simulate coupled ^{16}OH and ^{18}OH kinetics, we include two sets of four-well systems described above, each with unlabeled NO_2 but one with labeled ^{18}OH. The coupling reaction is $H(^{18}O)NO_2 \leftrightarrow HON(^{18}O)O$, which adds another well, $HON(^{18}O)O$, to the simulation. The labeled ^{18}ONO produced when this dissociates is always much less abundant than unlabeled NO_2, which allows us to simplify the simulation a bit, as discussed below.

In total, there are nine wells when we simulate ^{18}OH + ^{16}OH + NO_2, giving 16 transition states: seven transition states in the ^{16}OH + NO_2 four-well system, seven transition states in the ^{18}OH + NO_2 four-well system, one transition state for $H(^{18}O)NO_2$ scrambling to $HON(^{18}O)O$, and one transition state for $HON(^{18}O)O$ dissociation to OH + ^{18}ONO. We use the second set of four-well parameters in Table 1 for the corresponding energies here. For the critical energy of the isotopic scrambling (E_{TS3}), we use the value from our calculation shown in Table 1. We will present a sensitivity analysis for E_{TS3} below. The energy grain size is 30 cm^{-1}.

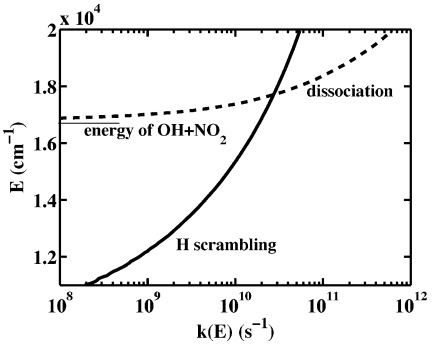

Figure 6. Microcanonical rate constants for H scrambling (to HONOO, solid line) and dissociation (to OH + NO_2, dashed line) of $HONO_2$. At all energies less than 1200 cm^{-1} above the (OH + NO_2), the H scrambling microcanonical rate constant is larger than the microcanonical rate constant for dissociation to OH + NO_2.

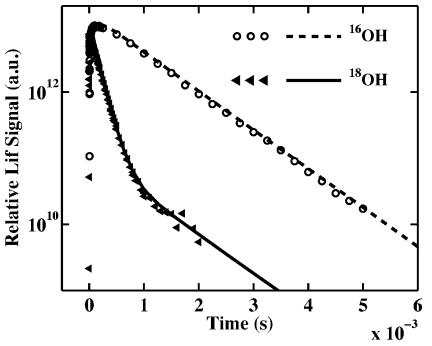

Figure 7. Simulation results from our nine-well master equation for conditions shown in Figure 3 in D'Ottone et al.[8] The collision frequency ω is 3×10^9 s^{-1}, $T = 298$ K, and $[NO_2] = 5.2 \times 10^{14}$ molecule cm^{-3}.

Figure 6 shows the microcanonical rate constants for H scrambling (to HONOO) and dissociation (to OH + NO_2) of $HONO_2$. The microcanonical rate constants $k(E)$ for H scrambling of $HONO_2$ are consistent with the values we calculated in our earlier work on ^{18}OH scrambling.[5] However, in that paper, we did not calculate the microcanonical rate constant for dissociation—instead we relied on an estimate of the high-pressure limits to estimate the average $k(E)$ for that path. Figure 6 presents $k(E)$ with a log scale to compare the microcanonical rate constants of H scrambling and dissociation more clearly; as with all of our microcanonical rate constant plots, we plot energy on the *y* axis to permit direct comparison with plots of the PES, where energy is also shown on the *y* axis. At all energies less than 1200 cm^{-1} above the (OH + NO_2), the H scrambling microcanonical rate constant is larger than the microcanonical rate constant for dissociation to OH + NO_2. This shows that the H scrambling reaction of $HONO_2$ is rapid, as we have argued in the past; however, the dissociation rate constant is within an order of magnitude of the scrambling rate constant over a wide range of energies. The question now is whether we can understand the full kinetics data, including the scrambling data, in this environment.

The simple answer is yes. Figure 7 shows the nine-well master-equation simulation for conditions identical to Figure 3 in D'Ottone et al.[8] The simulation results are almost perfectly

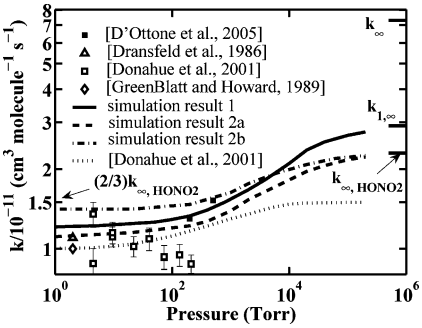

Figure 8. Rate coefficient of ^{18}OH loss vs pressure at 298 K, using parameters from the multiple-exponential kinetics and our computational scrambling barrier height without modification. The solid line is the full simulation, with $k_{\infty,i} = 2.3$, 1.5, and 3.5×10^{-11} cm^3 molecule^{-1} s^{-1} for the $HONO_2$, *trans*-HOONO, and *cis*-HOONO channels from OH + NO_2 association. The dashed line is for $k_\infty = 2.3 \times 10^{-11}$ cm^3 molecule^{-1} s^{-1} for the $HONO_2$ channel only (i.e., no *trans*-HOONO → $HONO_2$ isomerization is allowed). The two lines are parallel at low pressure but diverge when pressure increases. The dashed line has a high-pressure limit around 2.3×10^{-11}, while the solid line has a high-pressure limit ($k_{1,\infty}$) around 2.9×10^{-11}. The difference between the two high-pressure limits is caused by *trans*-HOONO conversion to $HONO_2$. The dash−dotted line has no isomerization and very low scrambling barrier, and it is parallel to the dotted line, which is the estimate of the pressure dependence presented in our earlier paper.[5] The symbols are the experimental results around 298 K.[5,8,37,38] The high-pressure limits for OH + NO_2 → $HONO_2$ and the total OH + NO_2 association rate constant are also shown.

consistent with the data in the figure, using the parameter set we obtained from the four-well simulations above. That parameter set was used without modification to constrain this simulation. This strongly suggests that those parameters are correct.

Given the excellent performance of the simulation, we can now consider the overall pressure dependence of the scrambling at 298 K. By varying the collision frequency in the simulation, we obtain a pressure dependence for the ^{18}OH disappearance shown in Figure 8. This is shown along with the literature data and a sigmoid function published in our earlier work.[5] Our complete simulation (shown as a solid black line) is very consistent with the data from D'Ottone et al.[8] The simulation is also reasonably consistent with the data from Dransfeld et al.,[37] Greenblatt et al.,[38] and Donahue et al.;[5] the current value is slightly higher than those data but within experimental uncertainty.

The sigmoid function published in our earlier work for the rate constant of ^{18}OH loss[5] is slower than the current simulation results for three reasons. The first reason is simply a difference in our assumed values for k_0 and k_∞ for the $HONO_2$ formation channel. The second two reasons are more interesting. One is scrambling via *trans*-HOONO, and the other is incomplete scrambling. Previously, we neglected isomerization of HOONO to $HONO_2$. To show the effect of this pathway, we turned off the isomerization in a second simulation, shown in Figure 8 with a thick dashed line (simulation 2a). In this case, the high-pressure limit for $HONO_2$ formation is the high-pressure limit for the direct pathway (2.2×10^{-11} cm^3 molecule^{-1} s^{-1}). In addition, lowering the scrambling barrier (TS3) to −4000 cm^{-1} (simulation 2b) permits total scrambling at all relevant energies (see below) and reproduces the earlier sigmoid, shifted to reflect the higher k_∞.

To directly assess the extent of scrambling in this reaction, we show in Figure 9 the ratio of pseudo steady state [HON(^{18}O)O] to [H(^{18}O)NOO] as a function of pressure and also the ratio at 200 Torr pressure as a function of energy (as usual, with energy

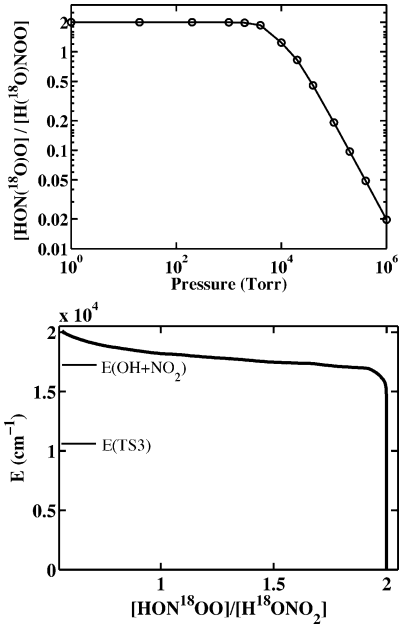

Figure 9. Ratio of pseudo steady state [HON(^{18}O)O] to [H(^{18}O)NOO] as a function of (a) pressure and (b) energy at 200 Torr. This ratio keeps constant at low pressure, with a value of 2, showing that isotopic scrambling is complete at low pressure. The ratio decreases rapidly with increasing pressure when pressure is larger than 2000 Torr. However, as shown in (b), the scrambling completes below the (OH + NO_2) dissociation limit, so OH isotopic scrambling is not complete, even though $HONO_2$ is.

on the *y* axis). The ratio remains at 2 from the low-pressure limit until the pressure increases to around 2000 Torr. This ratio is consistent with the statistical distribution of [HON(^{18}O)O] to [H(^{18}O)NOO], since there are two ^{16}O atoms but only one ^{18}O atom in the H(^{18}O)NO_2 molecule. While this indicates that scrambling is effectively complete, we must remember that most of the $HONO_2$ molecules are found below the dissociation threshold; in Figure 9b, we see that the statistical ratio is obtained below the dissociation energy but well above the scrambling barrier. Consequently, from the perspective of $HONO_2$ formation, scrambling is complete, but from the perspective of OH, the nascent H(^{18}O)NO_2 remains in excess and scrambling is thus not entirely complete.

Because the extent of scrambling is a major question here, we have also examined the sensitivity of these results to the transition-state energy (E_{TS3}). For our base-case model, we are using a computational result based on density-functional theory (B3LYP/6-31+G(d,p)), which is suspect for H atom transfers. The microcanonical rate constant for this reaction is also based on the geometries and frequencies from the simulation results. Figure 10a shows the simulation result in Figure 7, together with simulation results at different isotopic scrambling critical energies (E_{TS3}). Note that the base-case energy ($E_{TS3} = -130$ cm^{-1}) is slightly below the *cis*-HOONO energy, which serves as the reference energy for these simulations. The simulation is dramatically sensitive to E_{TS3} once the energy is raised by around 3000 cm^{-1} from the base-case simulation. However, there is some sensitivity to lowering the barrier height from the computational value, and conversely, the computational value is optimal. The lower energies, in blue and red, slightly overpredict the early slope in ^{18}OH, and the higher energy, in green, underpredicts that slope. Figure 10b shows the time dependence of the [HON(^{18}O)O] to [H(^{18}O)NOO] ratio for this same set of TS3 energies at a collision frequency of 10^9 Hz, and we see that indeed the pseudo steady state has not been

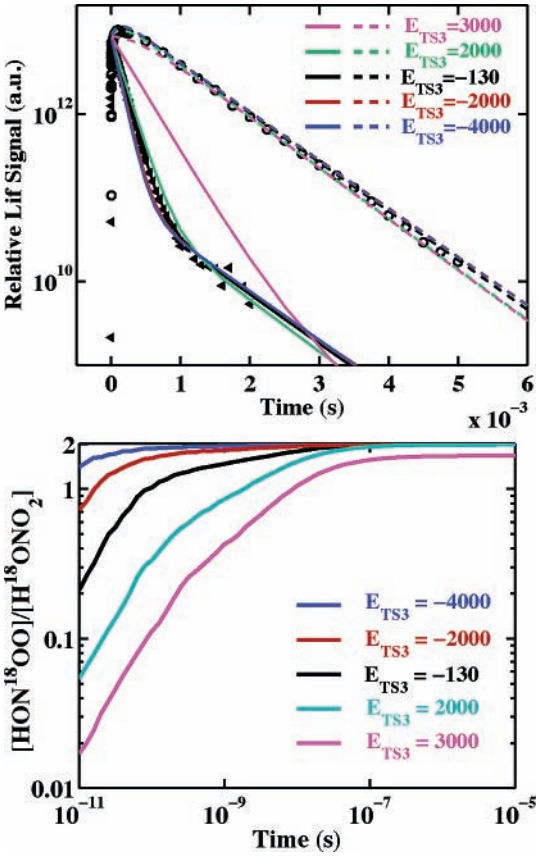

Figure 10. Sensitivity analysis showing the effect on the simulation results of varying the H atom scrambling barrier in $HONO_2$ (E_{TS3}) using a nine-well master equation. All the energies (in cm^{-1}) are relative to *cis*-HOONO; E(OH + NO_2) is 6500 cm^{-1} above this reference energy. The upper panel shows OH decay for both isotopomers over 0.006 s. Here, the solid lines are for ^{18}OH and the dashed lines are for ^{16}OH. The red lines are almost completely obscured by the blue lines. [^{16}OH] is minimally sensitive to E_{TS3}; [^{18}OH] is very sensitive to E_{TS3} only when E_{TS3} is more than 2000 cm^{-1} above E(*cis*-HOONO), but the computational value of E_{TS3} is clearly near the optimum. The lower panel shows the same sensitivity in the $HONO_2$ isotopomer ratio at $\omega = 10^9$ Hz, which is 2:1 for complete scrambling. For E_{TS3} below 3000 cm^{-1}, complete scrambling is eventually achieved, but well after the collision frequency until E_{TS3} is below -4000 cm^{-1}.

reached at 10^{-9} s unless E_{TS3} is below -4000 cm^{-1}, meaning that scrambling is not completed with a single collision, as suggested in D'Ottone et al.[8] While the sensitivity of the ^{18}OH kinetics to this value is slight, the outstanding agreement of our simulation and the D'Ottone et al. data without any modifications to our parameter set is encouraging.

Finally, D'Ottone et al.[8] also show the temperature dependence of the ^{18}OH disappearance rate as a function of pressure. The rate increases as the temperature decreases at high pressure. A significant portion of this temperature dependence is due to the increase of $HONO_2$ formation from HOONO isomerization at low temperature, which can cause a strong negative temperature dependence in the ^{18}OH removal rate even with individual values of k_∞ that are independent of temperature.

4.4. Nitrate Production from HO_2 + NO. Our final objective is to simulate $HONO_2$ production from the HO_2 + NO reaction using the same PES and parameters already presented. Experimental constraints are provided by the recent observations of $HONO_2$ formation from the HO_2 + NO reaction.[32] Those data reveal a significant $HONO_2$ yield at 200 Torr pressure of approximately 0.0015 at 300 K,[32] with a linear pressure dependence at lower pressure. This will constrain the

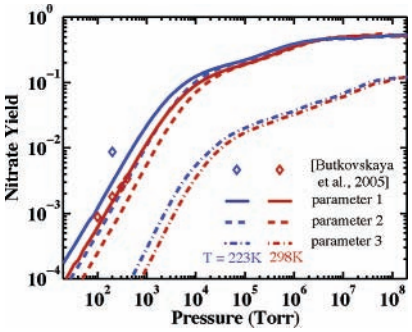

Figure 11. Pressure dependence of nitric acid production from the HO_2 + NO reaction for the HNO_3 PES presented in this paper using three parameter sets (see text). Set 1 has *trans*-HOONO largely isomerizing to *cis*-HOONO, while sets 2a and 2b have *trans*-HOONO largely isomerizing to $HONO_2$. Set 2b has a lower HO_2 + NO energy than set 2b, though both are within current uncertainty limits. The diamond markers represent experimental data from Butkovskaya et al.[32] The best fit (solid lines, set 2b) includes a relatively low *trans*-HOONO to $HONO_2$ isomerization barrier and a relatively low (HO_2 + NO) → (OH + NO_2) reaction enthalpy. These results quantitatively match the $HONO_2$ observations at 300 K and qualitatively reproduce the temperature dependence, though with less of a slope than the data. They are also consistent with observed *trans*-HOONO decay kinetics.[12]

choice between the 2 four-well parameter sets consistent with the OH + NO_2 data. To simulate $HONO_2$ production, we use the modeling framework from our earlier work on nitrate yields from RO_2 + NO[13] and the two parameter sets obtained from the four-well simulations. There is some uncertainty in the HO_2 reaction enthalpy for HO_2 + NO → OH + NO_2, which we shall address below.

In Figure 11, we show simulation results for the $HONO_2$ yield under three conditions. Using the first four-well parameter set from Table 2, we underpredict the observed $HONO_2$ yields by a factor of 10 (dashed−dotted lines, labeled "parameter 1"). With the second four-well parameter set, which has a low barrier to $HONO_2$, we are able to model $HONO_2$ yields similar to those observed (dashed lines, labeled "parameter 2a"). If we lower the (HO_2 + NO) energy from 7900 to 7400 cm^{-1} relative to *cis*-HOONO, then we obtain an excellent fit for nitrate yield at 300 K (solid lines, labeled "parameter 2b"). This (HO_2 + NO) energy is consistent with the computational value of Lohr et al. at B3LYP/6-311++G**.[24] Our simulations do show an increasing yield with decreasing temperature, but we show an increase of approximately a factor of 2 between 298 and 223 K whereas the data show an increase of approximately a factor of 4. We also attempted to simulate $HONO_2$ formation by eliminating direct dissociation of *trans*-HOONO to OH + NO_2 and maintaining a very low cis−trans isomerization barrier, consistent with the Ellison hypothesis.[34] We could not reproduce the data with those assumptions.

The falloff behavior for nitrate production shows a dual pressure dependence because of stabilization in both the HOONO and $HONO_2$ wells, with $HONO_2$ stabilization evident at low pressure ($<10^4$ Torr) and HOONO stabilization evident at intermediate pressure ($10^4 < p < 10^8$ Torr).[13] The data are clearly in the low-pressure regime where highly vibrationally excited $HONO_2$ is formed at the HO_2 + NO energy and then a small fraction is collisionally stabilized to generate the observed $HONO_2$.

In summary, two parameter sets based on a four-well model of the HNO_3 system are consistent with essentially all of the OH + NO_2 kinetic data, but added consideration of the yield of $HONO_2$ from HO_2 + NO breaks this symmetry in favor of a parameter set enabling rapid isomerization of *trans*-HOONO

to $HONO_2$ but inhibiting conversion of *trans*-HOONO to *cis*-HOONO. Furthermore, this model including $HONO_2$ formation from *trans*-HOONO reproduces the isotopic scrambling data in all its facets without any modification.

5. Discussion

5.1. Kinetics-based Results. The multiple-well model presented here (Table 2) is constrained by data, with computational results (Table 1) used primarily to set the parameter ranges. There are certain theoretical and/or computational findings, such as a barrier to *trans*-HOONO formation from OH + NO_2, a low isomerization barrier from *trans*- to *cis*-HOONO, and any formal transition state from a HOONO conformer to $HONO_2$, which we regard as insufficiently certain from a theoretical perspective to provide a firm constraint. Consequently, we have adopted a "data first" perspective to our modeling, seeking to find a model that is consistent with all of the available data. We have found one parameter set that comes very close to that objective. It successfully reproduces the biexponential OH decay reported by Hippler et al. and D'Ottone et al.,[6,8] it simultaneously reproduces the ($^{18}OH + NO_2$) isotopic scrambling data,[5,8,37,38] and it reproduces the $HONO_2$ yields from HO_2 + NO at 298 K.[32] Consistency is one thing, completeness is another; the PES is sufficiently complex that there may be other consistent solutions. However, within the parameter range we subjected to an exhaustive search, the current solution is the unequivocal winner.

The base-case model represented by the four-well parameters in Table 2 plus the scrambling barrier addressed in the nine-well results is quite highly coupled. The *trans*-HOONO intermediate is the key player in this coupling. There are three exit channels from this intermediate (four if one counts HO_2 + NO), and they are well correlated in terms of entropy and energy. The lowest barrier (TS2, from *trans*-HOONO to $HONO_2$) is relatively loose (high entropy), while the next lowest barrier (TS1, from *trans*- to *cis*-HOONO) is the tightest, with the lowest entropy. The highest barrier (dissociation to OH and NO_2) is very loose indeed. Consequently, the branching among these pathways is very sensitive to pressure and temperature. Because the $HONO_2$ barrier (TS1) is lower energy and higher entropy than the cis−trans barrier (TS2), isomerization to $HONO_2$ always exceeds isomerization to *cis*-HOONO. However, at high-temperature, dissociation to radicals dominates. If the cis−trans barrier were the lowest (which is commonly assumed), the reaction dynamics would be even more intricate, with each pathway dominating under specific pressure and temperature conditions.

We can make some general statements about the relationships among parameters and the degree of constraint on those parameters:

(1) The energies of (HO_2 + NO) and $HONO_2$ (relative to *cis*-HOONO) are not sensitive to the OH kinetics, while the energies of (OH + NO_2), *trans*-HOONO, TS1 (interconversion between *trans*- and *cis*-HOONO), and TS2 (isomerization from *trans*-HOONO to $HONO_2$) are very sensitive to the OH kinetics. The (HO_2 + NO) energy is sensitive to the nitrate yield data.

(2) The energy of (OH + NO_2) relative to the energy of *cis*-HOONO is the most critical property in the simulation of the biexponential kinetics. This is because the biexponential OH decay is caused by the dissociation of *cis*-HOONO in the experimental time scale, and the well depth of *cis*-HOONO determines its lifetime.

(3) Increasing E_{TS1} yields nearly the same results as decreasing E_{TS2}. The covariance is not smooth, but rather it is a "W" with two distinct minima. This is the reason that two optimal parameter sets are nearly identical except E_{TS1} and E_{TS2}. In the overall optimum, the rate constant for interconversion between *trans*- and *cis*-HOONO is small at all pressures, while the rate constant for *trans*-HOONO isomerization to $HONO_2$ increases with increasing pressure. If the interconversion rate between *trans*- and *cis*-HOONO intermediates increases, the isomerization barrier to $HONO_2$ must be increased to compensate.

(4) There are two limits to the four-well simulation that effectively collapse to the three-well simulation numerically.

(a) A very low barrier for *cis*−*trans*-HOONO isomerization. In this case, the critical energy for *trans*-HOONO isomerization to $HONO_2$ must be large and the rate constant for this reaction must be small. The effective high-pressure limit to HOONO formation is the sum of the *cis*- and *trans*-HOONO formation rates, and the overall equilibrium constant (and the biexponential kinetics) are dominated by *cis*-HOONO. This limit cannot reproduce the $HONO_2$ yield data.

(b) A high barrier for cis−trans isomerization, with *cis*-HOONO parameters equal to the three-well parameters in Table 2. In this case, E_{TS2} can be quite low and it is *trans*-HOONO and $HONO_2$ that are closely coupled; however, the coupling is not complete and the full dynamics must be considered. This is the case we have previously found to hold for $RONO_2$ formation, where it has several appealing characteristics. Most importantly, it provides a ready explanation for the low-temperature, high-pressure limit for nitrate yields of ∼50%.[13] In the current case of the HNO_3 PES, the total isomerization rate constant from *trans*-HOONO is in part constrained by the ^{18}OH isotopic scrambling data and in part constrained by $HONO_2$ yield data. The optimal parameter set is consistent with both, with the exception that the modeled temperature dependence for the $HONO_2$ yield is shallower than the observed temperature dependence. This means that our conclusions about the RNO_3 and HNO_3 PESs are essentially identical and that a single basic PES with only subtle variations (specifically the RO or HO energy) can explain the vast majority of the experimental data for all classes of nitrates.

(5) The critical energy for $HONO_2$ isotopic scrambling (E_{TS3}) is only loosely constrained by the data, but the density-functional barrier height for scrambling, which yields a mild inhibition of scrambling, is clearly preferred to either higher or lower barriers. A sensitivity analysis shows that E_{TS3} is certainly lower than 3000 cm^{-1} relative to *cis*-HOONO.

(6) The simulation results are not very sensitive to the high-pressure limits for OH + NO_2 association to *trans*- and *cis*-HOONO, while the high-pressure limit for OH + NO_2 association to $HONO_2$ is critical to the simulation result. Increasing $k_{\infty,HONO2}$ has the same effect as decreasing E_{TS2}. This is quite easy to understand: when E_{TS2} decreases, the rate constant of conversion from *trans*-HOONO to $HONO_2$ increases and the $HONO_2$ formation rate increases as well.

(7) The parameters we allowed to vary are very sensitive to the collision frequency ω and E_{down} used in master equation; we specified values for both rather than exploring this sensitivity because the overall conclusions about branching are not sensitive to these parameters and the selected parameters yield good fits to the data without modification. However, direct comparison with experimental or theoretical parameters must account for uncertainty due to these additional degrees of freedom. Increasing ω, increasing E_{down}, and decreasing the (OH + NO_2) energy relative to *cis*-HOONO have a similar effect on the simulation.

Nitric acid production from HO_2 + NO plays an important, confirmatory role in our simulations, but the data favor *trans*-

TABLE 3: Equilibrium Constants (cm^3 $Molecule^{-1}$) of HOONO at Different Temperatures

T (K)	475	430	413	350	300	250	220	ref
OH + NO_2 ↔ *cis*-HOONO	6.43×10^{-18}	6.48×10^{-17}	1.84×10^{-16}	2.39×10^{-14}	4.86×10^{-12}	1.45×10^{-8}	6.86×10^{-6}	this work
		6.21×10^{-17}			1.50×10^{-12}	1.24×10^{-9}	3.05×10^{-7}	Golden[7]
	9.1×10^{-18}	4.0×10^{-17}						Hippler[6]
			4.5×10^{-17}					D'Ottone[8]
OH + NO_2 ↔ *trans*-HOONO	1.05×10^{-19}	5.27×10^{-19}	1.07×10^{-18}	2.59×10^{-17}	7.99×10^{-16}	8.73×10^{-14}	3.73×10^{-12}	this work
		1.64×10^{-18}			5.28×10^{-15}	1.19×10^{-12}	1.01×10^{-10}	Golden[7]

HOONO isomerization to $HONO_2$ even without this final input. The observed sensitivity of $HONO_2$ yields to water vapor is also consistent with a chaperone mechanism in which H_2O in the HO_2−water complex is ejected from the nascent HOONO, taking with it some additional energy and thus reducing the energy of the excited $HONO_2$ formed when this intermediate isomerizes. Clearly, very high-pressure $HONO_2$ yield data would be incredibly useful, with and without water vapor, as they would constrain the asymptotic behavior of this system. Our modeling results, summarized in Figure 11, suggest that the high-pressure yield could be quite large (up to 50%), so at least the signal would not be small in these difficult experiments.

5.2. HOONO Observations. Recent observations of both *cis*-[9,10,12] and *trans*-[11,12] HOONO provide additional constraints on this system. The kinetic observations of Fry et al.[12] in particular appear to show that both conformers of HOONO are formed easily from OH + NO_2; the least stable conformer, *trans*-HOONO, is seen to significantly decay over the time scale of the observations, which will only come to pass if the source of this conformer is an even higher free-energy reservoir (OH + NO_2). While it is possible for high-energy *cis*-HOONO to generate transient *trans*-HOONO, this process would be very inefficient compared with *cis*-HOONO decomposition to radicals. At the same time, the Fry et al. data do show that thermalized *trans*-HOONO is quite short-lived, even at 230 K. What they do not reveal directly is the sink of *trans*-HOONO. This could be isomerization to either *cis*-HOONO or $HONO_2$. The observed nitric acid yields require a relatively low isomerization barrier from *trans*-HOONO to $HONO_2$ of 3750 cm^{-1}, which is consistent with the activation energy observed by Fry et al. of 2760 ± 1000 cm^{-1}.

When the *trans*-HOONO observations are considered in conjunction with the $HONO_2$ yield data from HO_2 + NO, a self-consistent conclusion emerges. Rapid isomerization of *cis*-HOONO (or tightly coupled HOONO) to $HONO_2$ is excluded by the observed biexponential kinetics, and yet some facile isomerization pathway is required by the data. As a consequence, we conclude that the PES most consistent with the broad array of experimental data is characterized by relatively separate conformers of HOONO and a facile isomerization of *trans*-HOONO to $HONO_2$.

In addition to being a key to understanding the unified data set, this secondary $HONO_2$ pathway is atmospherically important. At low pressure, it adds around 10% to $HONO_2$ formation, but this fraction increases with pressure as the mean energy of the decomposing HOONO decreases (this favors nitrate formation over dissociation to radicals), reaching around 26% at very high pressure. This factor is an important contributor to $HONO_2$ production at atmospherically relevant pressures and thus must be considered in the overall analysis of the reaction for atmospheric modeling purposes.

5.3. Thermal Kinetics. Table 3 shows the equilibrium constants for OH + NO_2 ↔ *cis*-HOONO and OH + NO_2 ↔ *trans*-HOONO at different temperatures extracted from our four-well master equation using our optimal parameter set. Several literature values are also shown in the figure for comparison.

TABLE 4: Fitted Parameters for the Rate Constant of $HONO_2$ and *cis*- and *trans*-HOONO Formation

	$k_0(T) = k_0^{300}(T/300)^{-n}$		$k_\infty(T) = k_\infty^{300}(T/300)^{-m}$		$F_c(T) = F_c^{300}(T/300)^{-}$	
	k_0^{300}	n	k_∞^{300}	m	F_c^{300}	q
$HONO_2$ (total)	1.8×10^{-30}	3.0	3.2×10^{-11}	0	0.4	0
$HONO_2$ (1 well)	1.6×10^{-30}	2.5	2.2×10^{-11}	0	0.5	0
HOONO (sum)	2.0×10^{-32}	3.0	5.5×10^{-11}	0	0.5	0
trans-HOONO	6.5×10^{-33}	3.0	1.1×10^{-11}	0	0.45	0
cis-HOONO	1.6×10^{-32}	3.0	4.4×10^{-11}	0	0.45	0

Our results for equilibrium constants of HOONO are reasonably consistent with the results by Golden et al., but our temperature dependence of equilibrium constant for OH + NO_2 ↔ *cis*-HOONO is larger, and the temperature dependence for OH + NO_2 ↔ *trans*-HOONO is smaller. For OH + NO_2 ↔ *cis*-HOONO, our result is greater than the results by Hipper et al, but these are the conditions and data modeled by Golden et al. as well, and so the difference can be attributed to the different mathematics of the assumed mechanisms and correspondingly different parameter sensitivities. For instance, Hippler et al. did not separate *trans*- and *cis*-HOONO in their analytical model, while both master-equation simulations do. The difference between our results and those of D'Ottone et al. at 413 K is more difficult to understand; however, as we have seen, our modeling results do reproduce other data and modeling results where the comparison can be made, and we also do reproduce the data from D'Ottone et al. using the same parameter set.

We also show thermal kinetics parameters in Table 4 using the standard "Troe" falloff parametrization. These parameters were obtained by fitting the output from the master-equation simulations to the parametrized falloff function.[44] The results are also summarized in a figure in the Supporting Information. The practical consequences of this work can be seen in the first two lines of the table, which show the effective rate constants for all channels leading to $HONO_2$ and the rate constants for only the direct channel to $HONO_2$. The low-pressure limiting rate constant is approximately 10% higher when all channels are considered, while the high-pressure limiting rate constant is 50% higher. Because the combined $HONO_2$ formation comprises two very different falloff curves, the overall falloff curve also is very broad, with a broadening factor $F_c = 0.4$.

6. Conclusions

We have modified the generic PES for RNO_3/HNO_3 presented in an earlier paper[13] and a multiple-well master equation to simulate biexponential and isotopic scrambling kinetics data for the OH + NO_2 reaction as well as $HONO_2$ yield data from HO_2 + NO. Given the complexity of the PES, there are multiple parameter sets that give good fitting results to portions of the data set, several of which have been explored in the literature previously, but we have found a single parameter set that is consistent with almost all of the features of the complete data set. On this basis, we can reach some general conclusions about the nature of this PES. These are listed in order of confidence.

First, isotopic scrambling in $HONO_2$ is rapid but not 100% complete at 300 K. Specifically, scrambling is complete with respect to $HONO_2$, but it occurs after one collision and at an intermediate energy below the OH + NO_2 dissociation limit. Consequently, the kinetic data do show sensitivity to the scrambling barrier height.

Second, it is certain that there are two distinct conformers of the HOONO intermediates; they have been isolated spectroscopically. It is also clear that both are formed relatively easily from OH + NO_2, and that the more stable conformer (*cis*-HOONO) is lost almost entirely back to OH + NO_2 (the biexponential kinetics require this).

Third, there is strong experimental evidence that *trans*-HOONO has a loss transition state much lower in energy than (OH + NO_2). Coupled with the evidence for $HONO_2$ formation from HO_2 + NO and also the scrambling data, the most probable identity for this sink is the *trans*-HOONO → $HONO_2$ isomerization. This conclusion is also consistent with the mechanism we have proposed for organic nitrate formation from the RO_2 + NO reaction.[13] The presence of this facile isomerization to $HONO_2$ influences $HONO_2$ production from both HO_2 + NO and from OH + NO_2, as in general the formation of *trans*-HOONO is a "back door" pathway to $HONO_2$.

The case presented here is strong but not ironclad. The available computational results are not completely consistent with our analysis, and it is very difficult to claim that this is the only solution consistent with the data, given the sheer complexity of the PES. However, the experimental constraints on the system are growing, and the bulk of the agreement between the model presented here and the experimental data is quantitatively very strong. We are thus gaining confidence that the overall conclusions are substantially correct.

Acknowledgment. This work is supported by Grant ATM-0446495 from the National Science Foundation. We thank Tony Hynes and Horst Hippler for sharing raw data for this paper and Tony in particular for extensive discussions throughout.

7. Appendix 1: Master-Equation Theory

Building a multiple-well master equation within the matrix formalism requires extensive attention to detail and very large matrixes. What follows is an outline of the essential details.

7.1. Master-Equation Formalism. The matrix form of the time-dependent population $\mathbf{N}(t)$ is

$$\frac{d\mathbf{N}}{dt} = [\omega(\mathbf{P} - \mathbf{I}) - \sum \mathbf{K}_i]\mathrm{N} \equiv \mathrm{MN} \tag{2}$$

in which $\mathbf{M} = \omega(\mathbf{P} - \mathbf{I}) - \sum \mathbf{K}_i$, $\mathbf{P}$ is the normalized energy transfer matrix, $\mathbf{I}$ is the unit matrix, ω is the collision frequency, and $\mathbf{K}_i$ is a matrix of unimolecular rate constants for the ith channel. The time-dependent solution of eq 2 is

$$\mathbf{N}(t) = \mathbf{U} \exp(\Lambda t)\, \mathbf{U}^{-1}\, \mathbf{N}(0) \tag{3}$$

where $\mathbf{N}(0)$ is the initial population vector of $\mathbf{N}$, $\mathbf{U}$ is the right eigenvector matrix of $\mathbf{M}$, and Λ is the diagonal matrix of eigenvalues of $\mathbf{M}$.

7.2. Two-well Master Equation. We can treat radical association and dissociation reactions, such as OH + NO_2 = $HONO_2$, as two-well systems: an $HONO_2$ well and an (OH + NO_2) "well".[40] If [NO_2] ≫ [OH], then the two-well master equation takes the same form as eq 2

$$\frac{d\mathbf{N}}{dt} = \mathbf{M}'\mathbf{N} \tag{4}$$

where $\mathbf{M}'$ is the transfer matrix describing energy transfer in $HONO_2$, its dissociation to OH + NO_2, and its formation from OH + NO_2. In this form, we assume that compounds in all bimolecular "wells" are in thermal equilibrium, with a canonical energy distribution; for this reason, the bimolecular "well" is treated with a single row and column in the matrix. The top left block ($m \times m$) of matrix $\mathbf{M}'$ is identical to the matrix $\mathbf{M}$ in eq 2. The top m elements of the right column (Φ_i) of $\mathbf{M}'$ are the source terms calculated by eq 5. The first m elements of the bottom row of $\mathbf{M}'$ are the microcanonical rate constants for dissociation of $HONO_2$, which provide the rate of $HONO_2$ dissociation to OH. Finally, the bottom right element (m+1,m+1) is $-k_\infty[NO_2]$, which gives the rate of OH loss to form $HONO_2$.

$$\Phi_i = k_\infty[C]g_i \tag{5}$$

where g_i is defined by eq 6, and k_∞ is the limiting high-pressure association rate constant of OH + NO_2.

$$g_i = \frac{k_i[\mathrm{NO_2}]_i \exp(-E_i/kT)}{\sum_i k_i[\mathrm{NO_2}]_i \exp(-E_i/kT)} \tag{6}$$

where k_i is the microcanonical rate constant, $[NO_2]_i$ is the NO_2 concentration at energy E_i, k is the Boltzmann constant, and T is the temperature. NO_2 maintains a Boltzmann distribution.

The full form of $\mathbf{M}'$ is shown below in eq 7, with the same solution shown in eq 3.

$$\mathbf{M}' = \begin{bmatrix} M_{11} & M_{12} & \cdots & M_{1m} & \Phi_1 \\ M_{21} & M_{22} & \cdots & M_{2m} & \Phi_2 \\ \vdots & \vdots & \ddots & \vdots & \vdots \\ M_{m1} & \mathrm{M_{m2}} & \cdots & M_{mm} & \Phi_m \\ k_1 & k_2 & \cdots & k_m & -\mathrm{k_\infty[NO_2]} \end{bmatrix} \tag{7}$$

7.3. Three-well Master Equation. The three-well system under consideration here consists of $HONO_2$, HOONO, and (OH + NO_2). This is the simplest form in our calculation. If [NO_2] ≫ [OH], then the three-well master equation has the same form as eq 4, with $\mathbf{M}'$ calculated by eq 8. The solution of the three-well master equation is the same as that shown in eq 3.

$$\mathbf{M}' = \begin{bmatrix} M_{11}{}^{a} & \cdots & M_{1m}{}^{a} & 0 & \cdots & 0 & \Phi_1{}^{a} \\ \vdots & \ddots & \vdots & \vdots & \ddots & \vdots & \vdots \\ M_{m1}{}^{a} & \cdots & M_{mm}{}^{a} & 0 & \cdots & k_y{}^{b} & \Phi_m{}^{a} \\ 0 & \cdots & 0 & M_{x,x}{}^{b} & \cdots & M_{x,y}{}^{b} & \Phi_1{}^{b} \\ \vdots & \ddots & \vdots & \vdots & \ddots & \vdots & \vdots \\ 0 & \cdots & k_m{}^{a} & M_{y,x}{}^{b} & \cdots & M_{y,y}{}^{b} & \Phi_{y-m}{}^{b} \\ k_1{}^{a} & \cdots & k_m{}^{a} & k_1{}^{b} & \cdots & k_{y-m}{}^{b} & -k_\infty[\mathrm{NO_2}] \end{bmatrix} \tag{8}$$

The superscripts a and b represent $HONO_2$ and HOONO separately in the matrix $\mathbf{M}'$ shown above. There are nine blocks

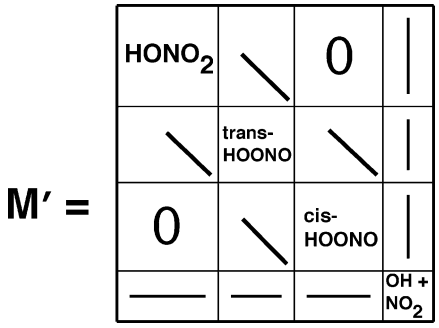

Figure 12. Simplified form of matrix **M′** in the four-well master-equation system. The diagonal blocks are for the four wells, which are the same as **M** in eq 2. In this figure, (|) means column vector, (−) means row vector, and (\) means diagonal matrix.

in the matrix **M′**. We define the block $\mathbf{B}_{i,j}$ as the *i*th row block and the *j*th column block. $\mathbf{B}_{i,i}$ represents the *i*th well, which has the same form as matrix **M** in eq 2 except the right bottom element. $\mathbf{B}_{i,j}$ ($i \neq j$) is a diagonal transfer array formed by the microcanonical rate constants in the diagonal, representing transformation from the *j*th well to the *i*th well. The number of rows in array $\mathbf{B}_{i,j}$ equals the size of matrix $\mathbf{B}_{i,i}$; the number of columns in array $\mathbf{B}_{i,j}$ equals the size of matrix $\mathbf{B}_{j,j}$. Consequently, the transfer matrix $\mathbf{B}_{i,j}$ is usually not square; however, the microcanonical rate constants sit in the diagonal starting from the lower-right corner cell of array $\mathbf{B}_{i,j}$ because all wells share a common highest energy.

The specific blocks in **M′** are as follows: The top-left block ($\mathbf{B}_{11}$ (elements (1,1) to (m,m))), representing the $HONO_2$ well, is the same as the matrix **M** in eq 2. The middle block ($\mathbf{B}_{22}$ (elements (m+1,m+1) to (y,y))), which is also the same as the matrix **M** in eq 2, represents the HOONO well. The bottom-right element ($\mathbf{B}_{33}$), which is the same as the bottom-right element in eq 7, represents OH disappearance by reaction with NO_2. All of the other six blocks contain the rate constants for conversion among the three wells: $\mathbf{B}_{12}$ ((1,m+1) to (m,y)) contains the microcanonical rate constants from HOONO to $HONO_2$ (well 2 to well 1) along the diagonal originating in the lower-right corner; $\mathbf{B}_{21}$ ((m+1,1) to (y,m)) contains the microcanonical rate constants from $HONO_2$ to HOONO (well 1 to well 2); $\mathbf{B}_{13}$ ((1,y+1) to (m,y+1)) is a $m \times 1$ vector, which is the source term from OH + NO_2 to $HONO_2$ calculated by eq 5; $\mathbf{B}_{23}$ ((m+1,y+1) to (y,y+1)) is a $(y - m) \times 1$ vector, which is the source term from OH + NO_2 to HOONO calculated by eq 5; $\mathbf{B}_{31}$ ((y+1,1) to (y+1,m)) is a $1 \times m$ row vector containing the microcanonical rate constants for dissociation of $HONO_2$ to OH + NO_2; $\mathbf{B}_{32}$ ((y+1,m+1) to (y+1,y)) is a $1 \times (y - m)$ row vector containing the microcanonical rate constants for dissociation of HOONO to OH + NO_2.

7.4. Four-well Master Equation. The four-well system separates HOONO into *cis*-HOONO and *trans*-HOONO. The four-well master equation has the same form as eq 4 with **M′** in a similar format as eq 8. The **M′** matrix is depicted in Figure 12. The solution of the four-well master equation is given by eq 3.

There are 16 blocks in the matrix **M′** for the four-well master equation. The diagonal blocks $\mathbf{B}_{11}$, $\mathbf{B}_{22}$, $\mathbf{B}_{33}$, and $\mathbf{B}_{44}$ are for $HONO_2$, *trans*-HOONO, *cis*-HOONO, and OH + NO_2 individually. All of the other 12 blocks are for conversions among these four wells, which have the same form as those above in the three-well master equation. Both $\mathbf{B}_{13}$ and $\mathbf{B}_{31}$ are zero matrixes since we assume that *cis*-HOONO cannot isomerize to $HONO_2$.

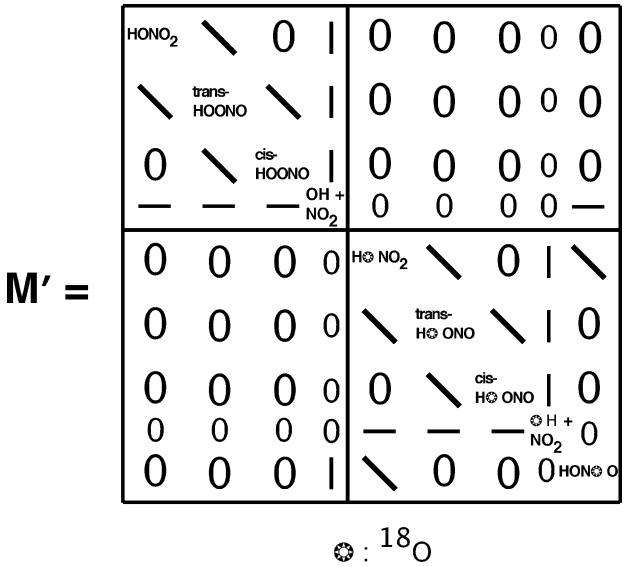

Figure 13. Simplified form of matrix **M′** in the nine-well master-equation system. The diagonal blocks are for the nine wells, which are the same as **M** in eq 2. In this figure, (|) means column vector, (−) means row vector, and (\) means diagonal matrix.

7.5. Nine-well Master Equation. The nine-well simulation of ^{18}OH isotopic scrambling consists of 2 four-well systems with a ninth well serving to couple them. The wells are $HONO_2$, *trans*-HOONO, *cis*-HOONO, (OH + NO_2) (the first four-well system), H(^{18}O)NO_2, *trans*-H^{18}OONO, *cis*-H^{18}OONO, (^{18}OH + NO_2) (the second four-well system), and HON(^{18}O)O (which couples the 2 four-well systems). The nine-well master equation also has the identical form of eq 4 with **M′** in a similar format as eq 8. The solution of the nine-well master equation is also identical by eq 3.

There are 81 blocks now in the matrix **M′** in the nine-well master equation. The diagonal blocks $\mathbf{B}_{11}$, $\mathbf{B}_{22}$, $\mathbf{B}_{33}$, $\mathbf{B}_{44}$, $\mathbf{B}_{55}$, $\mathbf{B}_{66}$, $\mathbf{B}_{77}$, $\mathbf{B}_{88}$, and $\mathbf{B}_{99}$ are for $HONO_2$, *trans*-HOONO, *cis*-HOONO, (OH + NO_2), H(^{18}O)NO_2, *trans*-H(^{18}O)ONO, *cis*-H(^{18}O)ONO, (^{18}OH + NO_2), and HON(^{18}O)O separately. All of the other 72 blocks are for conversion among these nine wells, which have a similar form as those above in the four-well master equation.

The simplified form of matrix **M′** is shown in Figure 13. There are four large blocks now in matrix **M′**: the top-left block (4×4) is for the (OH + NO_2) four-well system, which is the same as the matrix **M′** in Figure 12; the bottom-right block (5×5) is for the (^{18}OH + NO_2) system, which is similar to the top-left block. The difference is that there are five wells in this block, since we consider $HONO_2$ isotopic scrambling here and HON(^{18}O)O adds one more well to the previous four-well system. The top-right block (4×5) and bottom-left block (5×4) are both zero matrixes except for blocks $\mathbf{B}_{49}$ and $\mathbf{B}_{94}$, which represent the dissociation of HON(^{18}O)O to OH + N(^{18}O)O and OH + N(^{18}O)O reassociation to HON(^{18}O)O. For the sake of simplicity, we do not include an OH + N(^{18}O)O well in the matrix. Some N(^{18}O)O is formed from HON(^{18}O)O dissociation; we constrain this with a mass balance and allow the reaction back to HON(^{18}O)O but not the very minor HO(^{18}O)NO products.

8. Appendix 2: Energy Grain Size

We must make sure that the energy grain size in the simulation is small enough so that the results do not depend on the grain size. As we have addressed in the Results section, our default is a dual grain size (50 and 150 cm^{-1}) for the energy

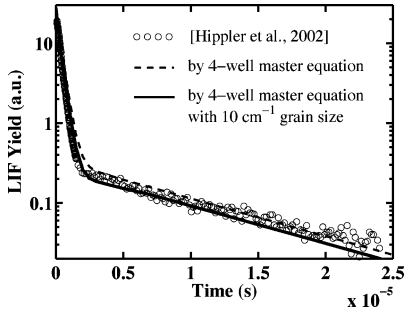

Figure 14. Fitting results for data by Hippler et al. at both 10 cm^{-1} grain size (solid line) and 50 cm^{-1} grain size (dashed line).

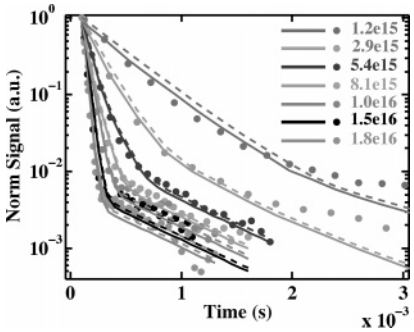

Figure 15. Fitting results for data by D'Ottone et al. at both 10 cm^{-1} grain size (solid lines) and 50 cm^{-1} grain size (dashed lines).

in all the simulations, with the finer grain near the transition-state energies.

We repeated the simulations from Figures 2 to 5 with the optimum parameter set at a much smaller grain size, 10 cm^{-1}, for all the energies. For the three-well case, the simulation results are nearly identical to Figures 2 and 3, which means that the grain size we used in the simulation is small enough and the simulation results are reasonable. But for the four-well case, the fine-grain results are a little different. The reason is pretty clear—as the number of wells increases, the number of transition states among the wells also increases and a finer energy grain size is needed to let the numerical results converge. The four-well simulation results at 10 cm^{-1} grain size with the optimum parameter set are shown in Figures 14 and 15 separately. In each case, the OH concentrations differ by about 10%. While this is a significant difference, it in no way changes our basic conclusions.

To test convergence for the 10 cm^{-1} grain size in the four-well case, we repeated the simulations for Figures 4 and 5 with the optimum parameter set at both 5 and 30 cm^{-1}. The results are almost the same as those for the 10 cm^{-1} grain size, showing that a 30 cm^{-1} grain size is sufficient for the four-well master-equation simulation. The optimal parameter sets do not change significantly with grain size. For the nine-well master-equation calculations, we use a 30 cm^{-1} grain size; no parameters are updated in these simulations, as the initial guesses based on the four-well simulation and our density-functional value for TS3 reproduce the experimental data.

9. Appendix 3: Thermal Kinetics

Fit results to master-equation simulations are shown in Figure 16. These fits use only the biexponential kinetics (i.e., the data used for the simulations in this paper) and thus do not make use of the vast literature on thermal OH + NO_2 kinetics at reduced pressure and many temperatures. They should thus not be considered to be a recommendation for atmospheric modeling.

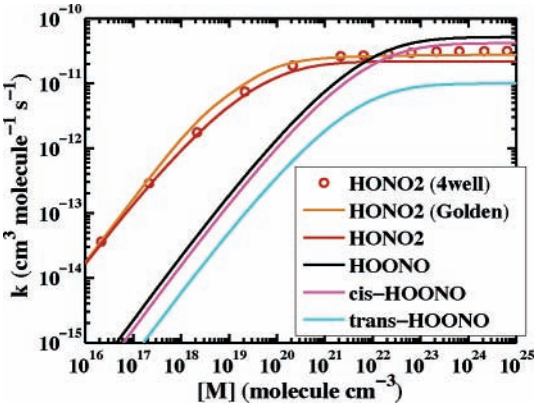

Figure 16. Thermal kinetic functions using the Troe falloff parameters shown in Table 4. The combined production of $HONO_2$ is shown with red circles, which rise progressively above the red curve, especially at high pressure where *trans*-HOONO formation leads to $HONO_2$ with high efficiency. The Golden results are shown in gold for comparison.

Supporting Information Available: Geometries and frequencies for all stable species and the transition state between *trans*- and *cis*-HOONO intermediates of the HO + NO_2 reaction system optimized at the B3LYP/6-31+G(d,p) level of theory by Gaussian98. This material is available free of charge via the Internet at http://pubs.acs.org.

References and Notes

(1) Johnston, H. *Science* **1971**, *173*, 517.
(2) Johnston, H. S. *Annu. Rev. Phys. Chem.* **1975**, *26*, 315.
(3) Logan, J. A.; Prather, M. J.; Wofsy, S. C.; McElroy, M. B. *J. Geophys. Res.* **1981**, *86*, 7210.
(4) Golden, D. M.; Smith, G. P. *J. Phys. Chem. A* **2000**, *104*, 3991.
(5) Donahue, N. M.; Mohrschladt, R.; Dransfield, T. J.; Anderson, J. G.; Dubey, M. K. *J. Phys. Chem. A* **2001**, *105*, 1515.
(6) Hippler, H.; Nasterlack, S.; Striebel, F. *Phys. Chem. Chem. Phys.* **2002**, *4*, 2959.
(7) Golden, D. M.; Barker, J. R.; Lohr, L. L. *J. Phys. Chem. A* **2003**, *107*, 11057.
(8) D'Ottone, L.; Bauer, D.; Campuzano-Jost, P.; Fardy, M.; Hynes, A. J. *Faraday Discuss.* **2005**, *130*, 1.
(9) Nizkorodov, S. A.; Wennberg, P. O. *J. Phys. Chem. A* **2002**, *106*, 855.
(10) Bean, B. D.; Mollner, A. K.; Nizkorodov, S. A.; Nair, G.; Okumuru, M.; Sander, S. P.; Peterson, K. A.; Francisco, J. S. *J. Phys. Chem. A* **2003**, *107*, 6974.
(11) Pollack, I. B.; Konen, I. M.; Li, E. X. J.; Lester, M. I. *J. Chem. Phys.* **2003**, *119*, 9981.
(12) Fry, J. L.; Nizkorodov, S. A.; Okumurab, M.; Roehl, C. M.; Francisco, J. S. *J. Chem. Phys.* **2004**, *121*, 1432.
(13) Zhang, J.; Dransfield, T. J.; Donahue, N. M. *J. Phys. Chem. A* **2004**, *108*, 9082.
(14) Anastasi, C.; Smith, I. W. M. *J. Chem. Soc., Faraday Trans.* **1976**, *72*, 1459.
(15) Wine, P. H.; Kreutter, N. M.; Ravishankara, A. R. *J. Phys. Chem.* **1979**, *83*, 3191.
(16) Donahue, N. M.; Dubey, M. K.; Mohrschladt, R.; Demerjian, K.; Anderson, J. G. *J. Geophys. Res.* **1997**, *102*, 6159.
(17) Fulle, D.; Hamann, H. F.; Hippler, H.; Troe, J. *J. Chem. Phys.* **1998**, *108*, 5391.
(18) Dransfield, T. J.; Perkins, K. K.; Donahue, N. M.; Anderson, J. G.; Sprengnether, M. M.; Demerjian, K. L. *Geophys. Res. Lett.* **1999**, *26*, 687.
(19) Brown, S. S.; Talukdar, R. K.; Ravishankara, A. R. *J. Chem. Phys. Lett.* **1999**, *299*, 277.
(20) D'Ottone, L.; Campuzano-Jost, P.; Bauer, D.; Hynes, A. J. *J. Phys. Chem. A* **2001**, *105*, 10538.
(21) Chakraborty, D.; Park, J.; Lin, M. C. *J. Chem. Phys.* **1998**, *231*, 39.
(22) Matheu, D. M.; Green, W. H. *Int. J. Chem. Kinet.* **2000**, *32*, 245.
(23) Troe, J. *Int. J. Chem. Kinet.* **2001**, *33*, 878.
(24) Lohr, L. L.; Barker, J. R.; Shroll, R. M. *J. Phys. Chem. A* **2003**, *107*, 7429.
(25) Barker, J. R.; Lohr, L. L.; Shroll, R. M.; Reading, S. *J. Phys. Chem. A* **2003**, *107*, 7434.

(26) Burkholder, J. B.; Hammer, P. D.; Howard, C. J. *J. Phys. Chem.* **1987**, *91*, 2136.
(27) Mcgrath, M. P.; Francl, M. M.; Rowland, F. S.; Hehre, W. J. *J. Phys. Chem.* **1988**, *92*, 5352.
(28) Li, Y.; Francisco, J. S. *J. Phys. Chem.* **2000**, *113*, 7976.
(29) Dixon, D. A.; Feller, D.; Zhan, C.; Francisco, J. S. *J. Phys. Chem. A* **2002**, *106*, 3191.
(30) Zhang, D.; Zhang, R. *J. Am. Chem. Soc.* **2002**, *124*, 9600.
(31) Zhao, Y.; Houk, K. N.; Olson, L. P. *J. Phys. Chem. A* **2004**, *108*, 5864.
(32) Butkovskaya, N. I.; Kukui, A.; Pouvesle, N.; Le Bras, G. *J. Chem. Phys. A* **2005**, *109*, 6509.
(33) Mcgrath, M. P.; Rowland, F. S. *J. Chem. Phys.* **2005**, *122*, 124312.
(34) Ellison, G. B.; Herbert, J. M.; McCoy, A. B.; Szalay, P. G.; Stanton, J. F. *J. Phys. Chem. A* **2004**, 7639.
(35) Smith, I. W. M.; Williams, M. D. *J. Chem. Soc., Faraday Trans.* **1985**, *81*, 1849.
(36) Forster, R.; Frost, M.; Fulle, D.; Hamann, H. F.; Hippler, H.; Schlepegrell, A. *J. Chem. Phys.* **1995**, *103*, 2949.
(37) Dransfield, P.; Lukacspaal, J.; Wagner, H. G. *Z. Naturforsch.* **1986**, *41* (11), 1283.
(38) Greenblatt, G. D.; Howard, C. J. *J. Phys. Chem.* **1989**, *93*, 1035.
(39) Barker, J. R. *Int. J. Chem. Kinet.* **2001**, *33*, 232.
(40) Holbrook, K. A.; Pilling, M. J.; Robertson, S. H. *Unimolecular Reactions*; John Wiley & Sons: New York, 1996.
(41) Kroll, J. H.; Sahay, S. R.; Anderson, J. G.; Demerjian, K. L.; Donahue, N. M. *J. Phys. Chem. A* **2001**, *105*, 4446.
(42) Reid, R. C.; Sherwood, T. K. *The Properties of Gases and Liquids*, 2nd ed.; McGraw-Hill: New York, 1966.
(43) Troe, J. *J. Chem. Phys.* **1977**, *66*, 4758.
(44) Troe, J. *Ber. Bunsen-Ges. Phys. Chem.* **1974**, *78*, 478.